ADVANCES IN ATMOSPHERIC SCIENCES, VOL. 30, NO. 5, 2013, 1491–1506

ENSO Indices and Analyses

WANG Zhiren*[1] (王志仁), WU Dexing[2] (吴德星), CHEN Xue'en[2] (陈学恩), and QIAO Ran[3] (乔 然)

[1]*Institute of Marine and Coastal Sciences of Rutgers University, New Jersey* 08901*, USA*

[2]*Physical Oceanography Laboratory, Ocean University of China, Qingdao* 266100

[3]*National Research Center for Marine Environmental Forecasts, Beijing* 100081

(Received 19 September 2012; revised 20 November 2012; accepted 21 November 2012)

ABSTRACT

New ENSO indices were developed and the spatial variability and temporal evolution of ENSO were analyzed based on the new indices and modeling experiments, as well as multiple data resources. The new indices, after being defined, were validated with their good diagnostic characteristics and correlation with wind and SST. In the analysis after the definition and validation of the new indices, ENSO feedbacks from wind, heat fluxes, and precipitation were spatially and temporally examined in order to understand ENSO variability and evolution with some emphasized points such as the interaction among the feedbacks, the role of westerly wind bursts and the transformation between zonal and meridional circulations in an ENSO cycle, and the typical pattern of modern ENSO.

Key words: ENSO, ENSO indices, Walker Circulation, westerly wind bursts, ENSO feedbacks

Citation: Wang, Z. R., D. X. Wu, X. E. Chen, and R. Qiao, 2013: ENSO indices and analyses. *Adv. Atmos. Sci.*, **30**(5), 1491–1506, doi: 10.1007/s00376-012-2238-x.

1. Introduction

ENSO is an important equatorial Pacific interannual signal in global climate (Grove, 1998). Related to general atmospheric circulations such as the Hadley (Hadley, 1735) and Walker (Walker, 1923) Circulations, the occurrence of El Niño has been related to stochastic forcing (Moore and Kleeman, 1999; Perigaud and Cassou, 2000; Boulanger, 2001). One such forcing is westerly wind bursts — the abrupt enhancement of westerly winds within the equatorial western Pacific Ocean with a speed of at least 7 m s^{-1} and a duration of 5–20 days (Latif et al., 1988; Harrison and Vecchi, 1997). Westerly wind bursts develop in response to twin cyclones (one on each side of the equator) (Keen, 1982), are related to a 30–60-day propagating within the Indian Ocean (Lau and Chan, 1986), and have been diagnosed as the essential condition for the occurrence and maintenance of El Niño events (Ding and Zhang, 2000). However, as we will show, the present study suggests that westerly wind bursts are dependent components of an ENSO cycle.

Because of its high SST, heavy rainfall, and strong latent heat flux, the western low-frequency SST variations within the warm pool are caused by surface latent heat and downward shortwave radiation fluxes (McPhaden and Hayes, 1991; Lau and Sui, 1997; Wang and Fang, 2000), although longer-spanning data are better for covering the seasonal cycle. Using long-term data analyses, numerical modeling experiments, and the new ENSO indices, it is demonstrated in this work that feedbacks from heat fluxes, precipitation, SST, and wind stress are spatially and temporally dependent. Dynamical and thermodynamical processes can provide opposite feedbacks on ENSO through cloud, though a phase difference exists. Latent heat and shortwave radiation fluxes mainly counteract one another, especially in mature El Niño and La Niña phases, reducing the feedback effects of these two important heat fluxes. Also, for the majority (70%–80%) of the time-space [i.e. (10°S–10°N, 120°–160°E, 1979–2002) and (5°S–5°N, 180°–100°W, 1979–2002)] examined in this study, variations for these feedbacks approximately represent only 20% of their magnitudes, and their SST contribution is less than 20% of maximum SST contributions. As a result, secondary

*Corresponding author: WANG Zhiren, zrwang@marine.rutgers.edu

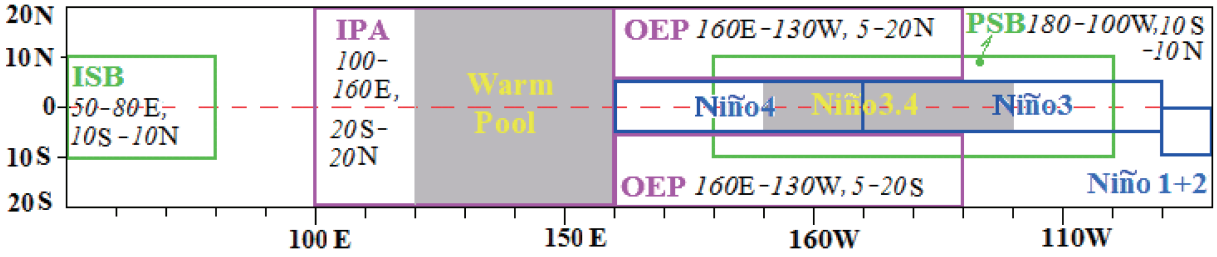

Fig. 1. A diagram of the typical tropical regions where ENSO and its factors change characteristically: the Indian subsiding branch of the Walker circulation (ISB) (10°S–10°N, 50°–80°E), the Indian-Pacific ascending branch (IPA) (20°S–20°N, 100°–160°E), the Pacific subsiding branch (PSB) (10°S–10°N, 180°E–100°W), the off-equator Pacific (OEP) (20°–5°S, 5°–20°N; 160°E–130°W), the Warm Pool (WP) (20°S–20°N, 120°–160°E), Niño 1+2 (0°–10°S, 90°–80°W), Niño 3 (5°S–5°N, 150°–90°W), Niño 4 (5°S–5°N, 160°E–150°W), and Niño 3.4 (5°S–5°N, 170°–120°W).

factors that may contribute to ENSO through some long-term accumulative process are still possible. Secondary factors include natural ones such as orbital effects and anthropogenic influences (e.g. Stenchikov and Robock, 1995; Cox and Jones, 2008; Lean and Rind, 2008; Wang et al., 2012).

Can an El Niño-like pattern of ENSO (warm climate) be permanently maintained? Wara et al. (2005) determined that during the early Pliocene Warm Period (∼4.5 to 3.0 m yrs before present) the eastern Pacific thermocline was deep and the average west-to-east SST difference across the equatorial Pacific was 0.6°C to 2.4°C, much like a modern El Niño pattern. Koutavas et al. (2002) found that the same average SST gradient during the Last Glacial Maximum (23 to 19 k yrs before present) was 0.9°C to 1.5°C less than that during the late Holocene (4.5 k yr to present) and displayed a persistent El Niño-like pattern within the tropical Pacific circulation. However, as determined in this study, Niño 1+2 SST changes inversely with the Walker Circulation intensity (WCI) to form a positive feedback in the Walker Circulation and conduces to maintain the La Niña-like pattern of modern ENSO (present paper). In a sense, the transformation between a La Niña phase and an El Niño phase is the transformation between zonal and meridional circulations, according to the climatologically-averaged winds. For example, during El Niño, zonal wind is weaker than normal. The zonal characteristic of the atmospheric and oceanic circulations conduces to maintain a La Niña-like pattern. The stable westward momentum accumulation of tropical ocean and atmosphere under the tidal forces provides a dynamic mechanism in maintaining the La Niña-like pattern of ENSO (Wang et al., 2012)[a].

The remainder of the paper is organized as follows. In section 2, the data are described and the regions of concentration for the ENSO study are defined. In sections 3 and 4, the new ENSO indices are introduced and compared to the classic southern oscillation indices (SOIs) via correlations with SST and wind. The ENSO prognostic characteristics of WCI for Niño SSTs and winds are given in section 5. A comprehensive ENSO analysis with new ENSO indices, data and numerical experiments is presented in section 6. Finally, a summary and discussion are provided in section 7.

2. Data resources and definition of regions

Data and their sources included the following: (1) the winds from the National Centers for Environmental Prediction (NCEP) reanalysis, geopotential height, air temperature, moisture, pressure, and sea surface heat fluxes provided by the National Oceanic and Atmospheric Administration (NOAA) and its Cooperative Institute for Research in Environmental Sciences; (2) QuickSCAT (an Earth observation satellite carrying the SeaWinds scatterometer) surface winds provided by the Ocean Vector Winds Science Team of the National Aeronautics and Space Administration (NASA); (3) indices of Niño SSTs, winds, and the Southern Oscillation provided by the NOAA/National Weather Service and the NCEP/Climate Prediction Center; (4) SST provided by the National Center for Atmospheric Research (NCAR); (5) Levitus salinity; and (6) CMAP (the Climate Prediction Center Merged Analysis of Precipitation) precipitation. Within the tropical Indian and Pacific Oceans, there are typical regions (Fig. 1) where ENSO and its factors change characteristically. In addition to classical Niño regions, new regions were added as follows: ISB, the Indian subsiding branch of the Walker circulation (10°S–10°N, 50°–80°E); IPA, the Indian-Pacific ascending branch (20°S–20°N, 100°–160°E); PSB, the Pacific

[a]Wang, Z., 2012: The Gravitation Between Earth and the Sun-Moon — A Tie or a Helping Hand? under revision.

subsiding branch (10°S–10°N, 180°W–100°W); OEP, the off-equator Pacific (20°–5°S and 5°–20°N, 160°E–130°W); WP, the Warm Pool (20°S–20°N, 120°–160°E).

3. Introduction to the new ENSO indices

In order to quantitatively describe characteristics of ENSO, new indices are introduced here. They are, the WCI (Wang et al., 2012), the position of the Walker Circulation (WCP), the intensity of the Hadley Circulation (HCI), the intensity of the warm pool (WPI), and the position of the cold tongue (CTP) using the mass streamfunction (for WCI and HCI), the position of the transition zone between the Indian and Pacific Walker Circulation cells (for WCP), the mean SST within the Warm pool (for WPI), and the equatorial position of a given isotherm (for CTP). Details are provided below.

3.1 *WCI and HCI*

This section will begin with an introduction to WCI and HCI and end with a physical explanation of them. Vertical vorticity has been widely used in atmospheric sciences (e.g. Holton, 1992; Wallace and Hobbs, 2006). The WCI and HCI are introduced using horizontal vorticity, written as

$$\boldsymbol{i}\left(\frac{\partial \rho w}{\partial y}-\frac{\partial \rho v}{\partial z}\right)+\boldsymbol{j}\left(\frac{\partial \rho u}{\partial z}-\frac{\partial \rho w}{\partial x}\right)\approx \boldsymbol{i}\,\frac{\partial^2 \Phi}{\partial z^2}+\boldsymbol{j}\,\frac{\partial^2 \Psi}{\partial z^2}\,, \tag{1}$$

after applying the relationships $\rho u=\partial\Psi/\partial z$ and $\rho v=-\partial\Phi/\partial z$ between the mass flux $\rho\boldsymbol{V}=\rho u\boldsymbol{i}+\rho v\boldsymbol{j}+\rho w\boldsymbol{k}$ (unit: kg s^{-1} m^{-2}) and the mass streamfunction Ψ or Φ (unit: kg s^{-1} m^{-1}) in the x–z or y–z plane and using quasi-horizontal motion (i.e. $|w|<<|u,v|$, the mass streamfunction is mainly from the horizontal current with vertical current omitted) that is applicable to large-scale atmospheric circulations. Furthermore, hydrostatic equilibrium ($\partial p/\partial z\approx-\rho g$) for large-scale atmospheric circulations is applied so that the mass streamfunctions Ψ and Φ could be derived in a p-vertical coordinate, as follows:

$$\psi(\lambda,\varphi_{\rm o},p,t)\equiv-\frac{1}{g}\int_{p_{\rm s}}^{p}u(\lambda,\varphi_{\rm o},p,t)dp\,, \tag{2}$$

$$\Phi(\lambda_{\rm o},\varphi,p,t)\equiv\frac{1}{g}\int_{p_{\rm s}}^{p}v(\lambda_{\rm o},\varphi,p,t)dp\,. \tag{3}$$

The mass streamfunction deviation ($\Psi_{\rm d}$) relative to the mass streamfunction for the mean zonal wind is as follows:

$$\psi_{\rm d}(\lambda,\varphi_{\rm o},p,t)\equiv-\frac{1}{g}\int_{p_{\rm s}}^{p}[u(\lambda,\varphi_{\rm o},p,t)-\frac{1}{\lambda_2-\lambda_1}\int_{\lambda_1}^{\lambda_2}u(\lambda,\varphi_{\rm o},p,t)d\lambda]dp\,. \tag{4}$$

For the individual Walker cell j (j =1 and 2 for the Indian and Pacific Ocean cells, respectively), the deviant mass streamfunction within its typical region ($p\in[p_1,p_2]$, $\lambda\in[\lambda_{{\rm w}j},\lambda_{{\rm e}j}]$) defines its WCI (marked with subscript j) that represents the mass stream function deviation in the x-z plane (kg s^{-1} m^{-1}), as follows:

$$\mathrm{WCI}_j(t)\equiv\frac{n}{(p_2-p_1)(\lambda_{{\rm e}j}-\lambda_{{\rm w}j})}\int_{p_1}^{p_2}\int_{\lambda_{wj}}^{\lambda_{ej}}\Psi_{\rm d}(\varphi_{\rm o},\lambda,p,t)d\lambda dp, \tag{5}$$

where $\lambda_{\rm w1}=60°$E, $\lambda_{\rm e1}=110°$E, $n=+1$ (for the Indian branch), $\lambda_{\rm w2}=170°$E, $\lambda_{\rm e2}=130°$E, and $n=-1$ (for the Pacific branch). The area-weighed mean of the Indian WCI1 and Pacific WCI2 is the general Walker Circulation Intensity,

$$\mathrm{WCI}\equiv\frac{(\lambda_{\rm e1}-\lambda_{\rm w1})\mathrm{WCI}_1+(\lambda_{\rm e2}-\lambda_{\rm w2})\mathrm{WCI}_2}{(\lambda_{\rm e1}-\lambda_{\rm w1})+(\lambda_{\rm e2}-\lambda_{\rm w2})}\,. \tag{6}$$

The HCI is defined as the mean mass streamfunction (kg s^{-1} m^{-1}) of Φ within the typical region $\{p\in[p_1,p_2],\,\varphi\in[\varphi_s,\varphi_n]\}$, where, as follows,

$$\mathrm{HCI}\equiv\frac{m}{(p_2-p_1)(\varphi_n-\varphi_s)}\int_{p_1}^{p_2}\int_{\varphi_s}^{\varphi_n}\Phi(\lambda_{\rm o},\varphi,p,t)d\varphi dp, \tag{7}$$

where $\varphi\in[\varphi_s=10°\mathrm{N},\,\varphi_n=20°\mathrm{N}]$ and $m=+1$ in the Northern Hemisphere; $\varphi\in[\varphi_s=20°\mathrm{S},\,\varphi_n=10°\mathrm{S}]$, and $m=-1$ in the Southern Hemisphere; and their mean denotes the overall HCI.

The terms $\boldsymbol{i},\boldsymbol{j},\boldsymbol{k}$ indicate the unit vectors, and u,v,w indicate the wind speed components (in m s^{-1}), respectively, in the x, y, and z directions; ρ is the air density (in kg m^{-3}); and g, λ, φ, and p are the gravitational constant (m s^{-2}), the longitude (°), the latitude (°), and the pressure (Pa), respectively. Typically, p_1 = 80 000 Pa and p_2 = 30 000 Pa; and $\varphi_1=5°$S, $\varphi_2=5°$N, $\lambda_1=50°$E, $\lambda_2=100°$W, $\lambda_{\rm o}=(\lambda_1+\lambda_2)/2$, $\varphi_{\rm o}=(\varphi_1+\varphi_2)/2$, and $p_{\rm s}$ = 100 000 Pa. Speed components can be averaged within given zones:

$$u(\lambda,\varphi_{\rm o},p,t)=\frac{1}{\varphi_2-\varphi_1}\int_{\varphi_1}^{\varphi_2}u(\lambda,\varphi,p,t)d\varphi\,,$$

$$v(\lambda_{\rm o},\varphi,p,t)=\frac{1}{\lambda_2-\lambda_1}\int_{\lambda_1}^{\lambda_2}v(\lambda,\varphi,p,t)d\lambda\,.$$

What do WCI and HCI represent? The scalars WCI and HCI are the mean mass streamfunctions and express the volumetric flow rate of the Walker Cell along

an x–z plane of thickness $L_y(\varphi_1 - \varphi_2)$ and the Hadley Cell along a y–z plane of thickness $L_x(\lambda_1 - \lambda_2)$, respectively. Computed from the mean circulation state in the large (typical) area above the planetary boundary layer (from 80 000 to 30 000 Pa), their values do not rely on the geometrical shapes of the circulation cells and are not limited to local properties such as surface winds. Approximately speaking, external forces ($\boldsymbol{F}$, the Earth's rotation [with angular velocity $\boldsymbol{\omega} = 1.458\times10^{-4}(\cos\varphi\boldsymbol{j} + \sin\varphi\boldsymbol{k})$], and air diversity ($\nabla \cdot \boldsymbol{V}$), as well as their vorticity all cause temporal and spatial variations of the WCI and HCI, based on their control equation:

$$\frac{\partial^2}{\partial z^2}\frac{d}{dt}(\boldsymbol{i}\,\Phi + \boldsymbol{j}\,\Psi) = \nabla \times [\rho(\boldsymbol{V} \times \boldsymbol{\omega} + F - \boldsymbol{V}\,\nabla \cdot \boldsymbol{V})]\,,$$

derived from the original momentum equation, mass conservation and Eq. (1).

3.2 *WCP, WPI, and CTP*

The Walker Cell position (WCP, unit: m) is defined as the mean meridional position of the zero-ψ_d belt (marked as ψ_do), because the signs of ψ_d are opposite for the Indian and Pacific branches, leading to the following:

$$\mathrm{WCP} \equiv \frac{\pi R_\mathrm{e}\cos\varphi_\mathrm{o}}{180(p_2 - p_1)}\int_{p_1}^{p_2}[\lambda(\varphi_\mathrm{o}, p, \psi_\mathrm{do}, t) - \lambda_\mathrm{po}]dp\,, \tag{8}$$

where λ_po is the reference value (it is set as the value of WCP when the Walker cell approaches the most western position). The value can be 118.125°E and 105.625°E, based on the monthly and weekly wind from 1950 to 2007, respectively. In numerical calculations, $\psi_\mathrm{do} \in [-2.5\%\max\{|\Psi_\mathrm{d}|\}, 2.5\%\max\{|\Psi_\mathrm{d}|\}]$, and the Earth's radius is $R_\mathrm{e} \approx 6\,371\,000$ m.

The intensity of the warm pool (WPI) is defined as the area integration of SST whose value is no less than 28.5°C within a 100°–160°E latitudinal range, as follows:

$$\mathrm{WPI}(t) \equiv_{\Omega_a} \mathrm{SST}(s,t)ds\,. \tag{9}$$

Here, Ω_a is the region where the SST is no less than 28.5°C and its longitude is within 100°–160°E.

The stronger the cold tongue, the lower SST is within the cold tongue area, which relates to the position of the cold tongue (CTP) defined as the mean zonal position of an isotherm SSTo within a latitudinal belt of $\varphi \in [\varphi_1, \varphi_2]$, as follows:

$$\mathrm{CTP}(t) \equiv \frac{R_\mathrm{e}}{\varphi_2 - \varphi_1}\int_{\varphi_1}^{\varphi_2}\lambda(\varphi, \mathrm{sst_o}, t)d\varphi\,. \tag{10}$$

Here, $\mathrm{sst_o} \in [24.75°\mathrm{C}, 25°\mathrm{C}]$, and $\varphi \in [15°\mathrm{S}, 0°]$.

4. The integrity of atmospheric circulation and a correlation comparison

The WCI, WCP, HCI, WPI, and CTP represent different aspects of atmospheric circulation during ENSO. A high correlation among these aspects displays the integrity of atmospheric circulation (see section 6). For example, based on monthly data for the period 1950–2007, the WCI in both the Indian and Pacific Oceans changed simultaneously with a highly positive correlation of 0.882 — the same for the HCI in both the Northern and Southern Hemispheres with a high simultaneous positive correlation of 0.776. WCI and HCI changed in an opposite manner with a negative correlation of −0.636, with the WCI lagging by approximately one month. The WCI and the WCP changed oppositely with a negative simultaneous correlation of −0.405. A highly positive correlation existed between WCI and the meridional gradient of SST and the meridional gradient of shortwave radiation in the Niño3.4, 0.808 and −0.731, respectively, with the WCI lagging by one month. WCI and WPI were 46.2% correlated, the WCI and CTP were −88.5% correlated, and so on (rows 1–8 of Table 1; detailed analysis provided in section 6). In this study, all the given correlation coefficients with our newly developed indices have a confidence level above 95%. The confidence interval was examined via the matlab (v7.11.0) functions "corr" and "corrcoef", using an asymptotic normal distribution and Student's t-distribution (both sides), respectively, and via correlation coefficients and effective degrees of freedom (Emery and Thomson, 1998) computed by Chelton's formula (Chelton, 1983).

Among the new ENSO indices, the WCI was chosen as a typical ENSO index for the correlation comparison with classic Southern Oscillation indices. The WCI is independent of the geometry of the Walker circulation cell and local atmospheric or oceanic states. As compared to classic Southern Oscillation indices, the WCI generally has a higher correlation with SST and wind (Table 2), as follows: −0.72 versus −0.26 for correlation with Niño 1+2 SST; −0.75 versus −0.47 for correlation with Niño3 SST; −0.79 versus −0.65 for correlation with Niño3.4; −0.42 versus −0.65 for correlation with Niño4 SST; 0.66 versus 0.56 with the 85 000-Pa zonal wind averaged within 5°N–5°S and 135°–180°E; and 0.57 versus 0.39 with the 20 000-Pa zonal wind averaged within 5°N–5°S and 165°–110°W, based on monthly data from 1951–2007 for Niño SSTs or from 1979–2007 for zonal winds provided by the NOAA/National Weather Service and the NCEP/Climate Prediction Center. Therefore, the WCI may better express the ENSO properties for general atmospheric circulations.

5. ENSO prognostic characteristics of WCI for Niño SSTs and winds

The WCI has good ENSO prognostic characteristics for SST and winds, in addition to its greater correlation with Niño SSTs and winds. Eighteen El Niño years (17 El Niño events) and 19 La Niña years (13 La Niña events) from 1950 to 2007 were analyzed. Within each of the El Niño / La Niña years, Niño3.4 SSTA (SST anomaly, relative to climatological mean SST for the period 1971–2000) was $\geqslant 0.5^{\circ}$C / $\leqslant -0.5^{\circ}$C continuously for five months or longer (Fig. 2a, El Niño years: 1951, 1957, 1963, 1965, 1968, 1969, 1972, 1976, 1977, 1982, 1986, 1987, 1991, 1994, 1997, 2002, 2004, and 2006; La Niña years: 1950, 1954, 1955, 1956, 1964, 1967, 1970, 1971, 1973, 1974, 1975, 1984, 1985, 1988, 1995, 1998, 1999, 2000, and 2007). The rest of the years from 1950 to 2007 are referred to as normal years.

A clear warm-cold phase relationship exists between the WCIa (WCI anomaly, relative to climatological mean WCI for the period 1971–2000) and the Niño3.4 SSTA. For interannual variability with seasonality deducted (Fig. 2a), each cold Niño3.4 SSTA phase (i.e., SSTA $< 0^{\circ}$C) corresponded to a cold WCIa phase (i.e., WCIa > 0). Each warm Niño3.4 SSTA phase (i.e. SSTA $>0^{\circ}$C) corresponded to a warm WCIa phase (i.e. WCIa <0) with a high level of correlation (-0.76), based on monthly NCEP reanalysis data for the period 1950–2007. For seasonality in the WCI and SST, each summer the WCIa reached its maximum positive intensity while during the winter the WCIa reached a maximum in negative intensity (Fig. 2c). Prior to each of the 17 El Niño events for the period 1950–2007 a clear WCIa-prelude was determined for the occurrence of El Niño (i.e. the period of time when the WCIa reached extreme positive intensity until the time the next El Niño began with Niño3.4 SSTA reaching to 0.5°C), which led to El Niño prediction using the WCI. Preludes lasted between two and twelve months (mean: 8.8). In 13 cases there was not an accompanying warm SSTA phase (Fig. 2a). After reaching its maximum, the WCIa fell below zero and soon afterward it bounced back above zero, indicating the instability of the Walker circulation after reaching its maximum intensity. The phase-length and the amplitude of the WCIa corresponded well with ENSO (Figs. 2b and c). For 18 El Niño years, the negative WCIa phases lasted longer (7.5 months on average) and had larger amplitudes than during normal years. In contrast, during the 19 La Niña years, negative WCIa phases were shorter (1.5 on average) and had smaller amplitudes than during normal years. Positive WCIa phases lasted around 4.5, 8.5, and 7.5 months annually for El Niño, La Niña, and normal years, respectively. La Niña lasted the longest on an annual basis (>6 months) during an ENSO cycle (Figs. 2b and c).

The phase relationship between the WCI and surface zonal winds (including westerly wind bursts) was

Table 1. Correlations among the newly developed ENSO indices and ENSO factors (confidence level >95%) based on monthly NCEP reanalysis 1950–2007 for the correlations in rows 2–9 and monthly NCEP reanalysis and model simulation 1979–2003 for the correlations in rows 10–22.

Correlation with WCI (except correlations in rows 2-3)			Phase (month)
Indian and Pacific WCI		0.882	simultaneously
Northern and Southern HCI		0.776	simultaneously
HCI		−0.636	WCI lags 1
WCP		−0.405	WCI lags 0
Poleward ascendant of SST in Niño3.4		0.808	WCI lags 1
Poleward ascendant of shortwave in Niño3.4		−0.731	WCI lags 1
WPI		0.462	WCI lags 3
CTP		−0.885	WCI leads 1
Total heat	WP	−0.577	WCI leads 3
		0.269	WCI lags 10
	Niño3.4	0.884	WCI lead 1
Latent heat	WP	0.615	WCI lags 3
	Niño3.4	−0.808	WCI lags 1
Shortwave radiation	WP	−0.808	WCI leads 1
	Niño3.4	0.769	WCI leads 1
Sensible + longwave	WP	0.692	WCI lags 2
	Niño3.4	−0.538	WCI lags 3
Precipitation	WP	0.885	WCI leads 2
	Niño3.4	−0.885	WCI lags 0
Wind convergence	WP	0.654	WCI lags 3
	Niño3.4	−0.769	WCI lags 0

Table 2. Correlation comparison of the different ENSO indices (WCI, SOIe, SOIa, and SOIs) with SST and zonal wind. The values listed under the ENSO indices are the correlation coefficients. The data applied were monthly Niño SSTs (1951–2007) and zonal winds (1979–2007) from NOAA/National Weather Service and NCEP/Climate Prediction Center.

SSTs/Wind	Region	WCI	SOIe	SOIa	SOIs
Niño SSTs	Niño1+2	−0.72	−0.28	−0.26	−0.26
	Niño3	−0.75	−0.53	−0.47	−0.47
	Niño3.4	−0.79	−0.70	−0.65	−0.65
	Niño4	−0.42	−0.66	−0.65	−0.65
	Total mean	−0.67	−0.54	−0.51	−0.51
Zonal wind (5°N–5°S)	135°–120°W at 85 000 Pa	0.39	0.42	0.44	0.44
	175°–140°W at 85 000 Pa	0.70	0.78	0.72	0.72
	135°–180°E at 85 000 Pa	0.66	0.63	0.56	0.56
	165°–110°W at 20 000 Pa	0.57	0.46	0.39	0.39
	Total mean	0.58	0.57	0.53	0.53

Notes: SOIa/SOIs: The difference in the sea level pressure anomaly/standardized sea level pressure between Stations Tahiti and Darwin.
SOIe: The standardized sea level pressure difference between equatorial Indonesia (5°N–5°S, 90°–140°E) and the equatorial Eastern Pacific (5°N–5°S, 130°– 80°W).

checked using the Lanczos filter and a correlation, with similar results for the NCEP (columns 1 and 2 of Fig. 3) and QuickSCAT winds (columns 3 and 4 of Fig. 3).

For lower-frequency (i.e. the period of maintenance was longer than 10 weeks following a low-pass filter) WCI and zonal winds, the simultaneous correlation (the first row in columns 1 and 3 of Fig. 3) ranged from −0.8 to 0.7 and mainly exhibited an annual mode with hemispheric characteristics. The Walker circulation was typically intensified during summer months corresponding with intensified westerlies in the 5°–15°N latitude band over the Indian Ocean, but also with intensified easterlies (weakened westerlies) in the 5°–15°S latitude band over the Pacific. The inverse situation was a weakened Walker circulation during winter months. The low-frequency correlation between the WCI and zonal winds was persistently significant on an annual scale in each of the analyzed zones. The Walker circulation intensifies approximately 30 weeks before or 25 weeks after the westerlies in the 5°–15°S latitude band (the second row in columns 1 and 3 of Fig. 3), and last for an approximate one-year period. The intensified Walker circulation corresponds to stronger westerlies in the Indian Ocean, but to stronger easterlies in the Pacific Ocean within the 5°N–5°S latitude belt (the third row in columns 1 and 3 of Fig. 3). For the equatorial westerlies to extend eastward to approximately 155°E, the Walker circulation must intensify around 30 weeks prior to or roughly 25 weeks afterward. Within the 5°–15°N latitude band, the Walker circulation leads to a westerly intensification by ∼6.5 to ∼9.4 weeks, depending on different wind resources (the fourth row in columns 1 and 3 of Fig. 3).

For higher-frequency (i.e. the period of maintenance is shorter than 10 weeks following a high-pass filter) WCI and westerly wind bursts, the simultaneous correlation (the first row in columns 2 and 4 of Fig. 3), ranging from −0.6 and 0.6, demonstrates WCI-associated zonal, high-frequency wind oscillations in response to an intensified Walker circulation. The seasonality of ENSO could still be seen from the spatial correlation distribution, but there was no temporally persistent correlation between the WCI and winds within each of the checked zones (the second, third, and fourth rows in columns 2 and 4 of Fig. 3). Instead, a reliable correlation only existed for a few weeks prior to and after the maximum WCI. The Walker circulation reached its maximum intensity in roughly 2–4 weeks (2.3 weeks according to NCEP wind, and 3.6 weeks according to QuickSCAT wind) prior to a westerly wind burst. The weakest Walker circulation coincided with the maximum westerly, indicating that high-frequency Walker-circulation oscillators lead to westerly wind bursts when the Walker circulation is unstable. Both Walker circulation cells over the Pacific and Indian Oceans move eastward as they become the weakest (negative correlation between the WCI and the WCP, as stated in section 4 and shown in Table 3). That the high-frequency westerly changed with WCP can be demonstrated in a weekly averaged WCP and zonal wind within 5°S–5°N, for example at the beginning of two El Niño events that started in June 2002 and August 2006, respectively (Fig. 4). Prior to the occurrence of the El Niño events, WCP increased with Walker circulation moving eastward and becoming weaker. Concurrent weakening and the eastward propagation of the Pacific Walker cell corresponding with the weakening and eastward propagation of the Indian Walker cell permit the high-and-low-frequency

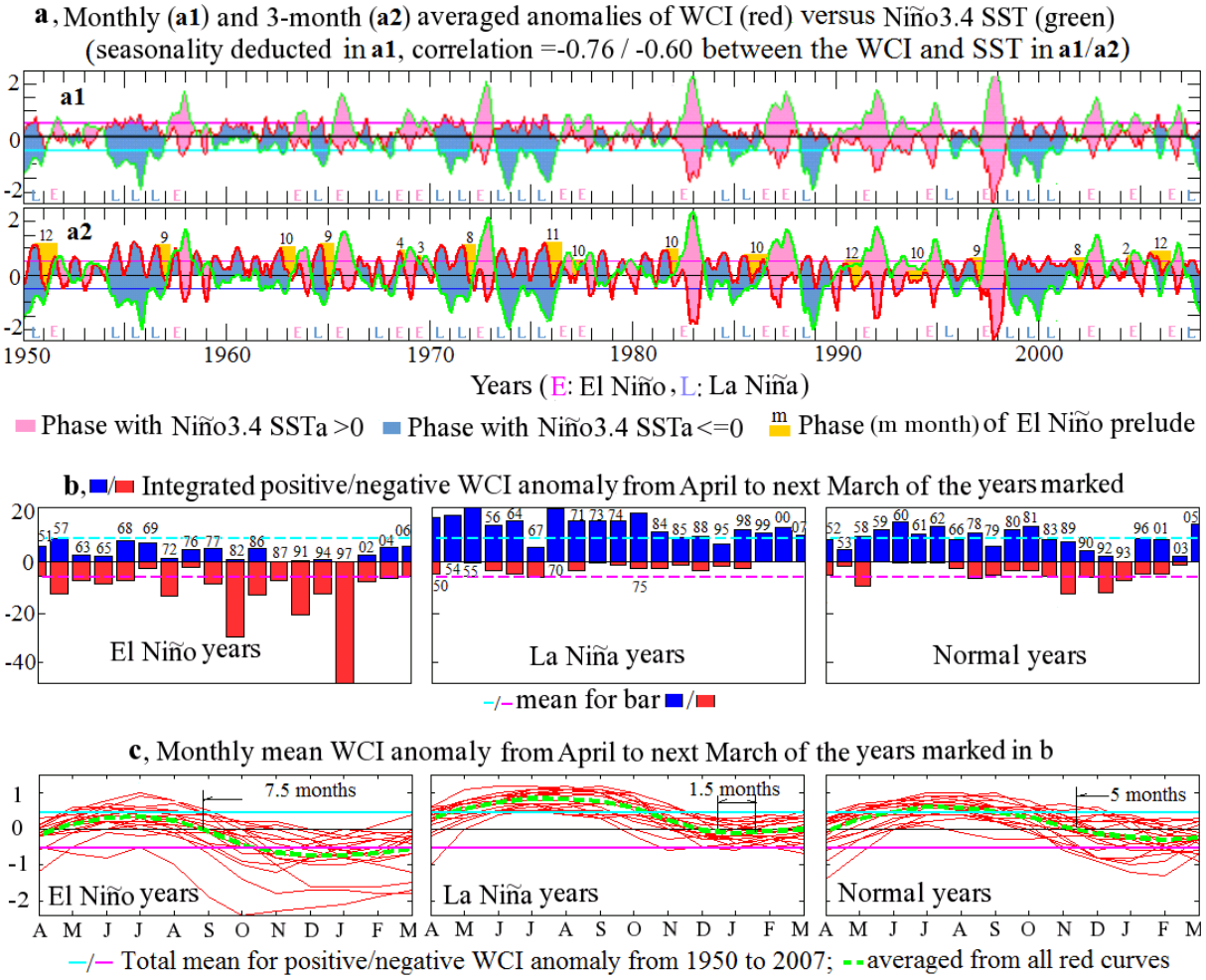

Fig. 2. The ENSO-diagnostic character of the WCI, as follows: (a) a significant prelude to and a high correlation with Niño3.4 SST; (b) a variation in the accumulative intensity; and (c) a change of phase length for El Niño versus La Niña years [an El Niño/La Niña year is defined as a year from April to the following March where the 3-month running mean Niño3.4 SSTA is always above 0.5°C or always lower than −0.5°C, as shown in (a) and (b)]. The units for SSTA are °C, and $\times 10^4$ kg s^{-1} m^{-1} for WCIa.

westerly from the Indian branch to spread eastward toward the Pacific.

6. ENSO feedback analysis using numerical experiments, new ENSO indices, and data

In this section we outline the comprehensive analysis of ENSO feedbacks using a simulation, new ENSO indices, and the data introduced in section 2. The Lamont Ocean-AML (atmospheric mixed layer) Model (LOAM) was applied in order to simulate global tropical climate for the period 1979–2002. LOAM was developed using the original Gent-Cane model (Gent and Cane, 1989), a primitive equation ocean circulation model that includes the heat flux formulation of Seager and Blumenthal (1994) and the mixed layer formulation of Chen et al. (1994). At its core, LOAM uses the hydrostatic balance, the rigid-lid approximation, the fourth-order centered differential in the horizontal, the fourth order temporal Lorenz cycle (Lorenz, 1971) (for high accuracy and low numerical diffusivity), the Shapiro filters (Shapiro, 1970), and a convective adjustment with wind stirring by assuming Richardson-number-dependent mixing. Model calculations were performed on a stretched A-grid with a 50–200-km horizontal resolution covering a 20°S–20°N latitude zone, 28 vertical layers, and a time step of 30 minutes. For the numerical experiments carried out in this study, the atmospheric mixed layer was treated simply as one layer within which the computed and observed surface atmospheric variables (wind, temperature, precipitation, and heat fluxes) were coupled directly with oceans. The model inputs were the following: (1) NCAR SST; (2) CMAP precipitation; (3)

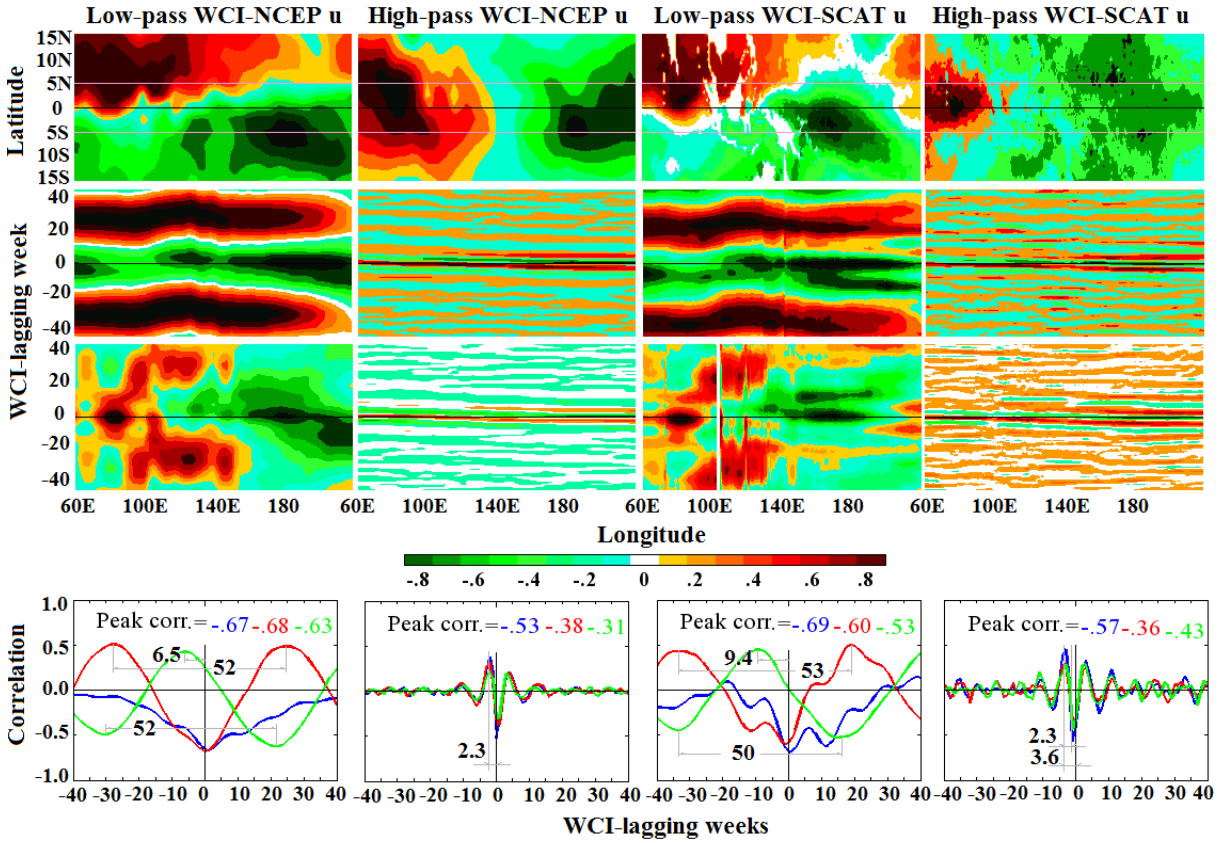

Fig. 3. Correlation between surface zonal winds and WCI at a lower frequency (the period of maintenance was longer than 10 weeks following the low-pass filter; first and third columns) and a higher frequency (the period of maintenance was shorter than 10 weeks following the high-pass filter; second and fourth columns). The first row displays simultaneous correlations at individual spatial points, and the second and third rows display WCI-lagging correlations between WCI and winds averaged within 5°S–5°N and 5°–15°S , respectively. The curves in the fourth row display WCI-lagging correlations between the WCI and winds averaged within (5°S–5°N, 140°E–140°W; blue), (5°–15°S, 140°E–140°W; red) and (5°–15°N, 140°E–140°W; green). Winds were obtained from daily NCEP reanalysis (1950–2007; first and second columns) and QuickSCAT (24 Jul 1999–2007; third and fourth columns).

Levitus salinity; and (4) NCEP reanalysis air temperature, moisture, wind, geopotential height, and sea surface heat fluxes. Longwave, sensible, and latent heat fluxes were computed using LOAM. Seven different cases were tested. For the comprehensive case (case7), all of the following factors were included: wind stress (F1), total heat flux (F2) that included latent heat flux (F3), shortwave radiation (F4) and longwave radiation plus sensible heat flux (F5), and precipitation (F6). A "case$N$" was used to evaluate a contribution (e.g. SST) from a factor FN (N=1–6). In order to see what a difference in contribution the factor FN could make in a comprehensive environment (i.e. the case7 that included all tested factors), case$N$ was defined as the contribution from case7 minus that from a case that included all tested factors, but not FN. Simply speaking, case$N$ tested the difference between the factor FN being included in the modeling, and not being included. The following analogy can be made: an investigator decides to test the roles of the left hand of a robot having two eyes, two hands and two legs (six parts in total, equivalent to the six tested "factors"). The robot can move nine books with the six parts, but moves seven books without the left hand. From this, the investigator is able to say the left hand helps to move two more books. In our numerical experiments, we also designed case$N$ in another way that could not express the contribution from a factor FN in the comprehensive environment.This method, whose results were not included in this study, involved designing a basic case that was driven by climatological means, and then case$N$ was designed as the basic case plus FN to test the contribution from factor FN. Returning to the above analogy, the robot cannot move any books without the six parts, but the robot can move one book with the left hand added. From

Table 3. Summary of circulations and the WCI-feedback between La Niña and El Niño phases, based on the model simulation and data reanalysis.

During La Niña:
- Walker Circulation intensifies and migrates westward;
- Hadley circulation becomes weaker and less meridionally extended;
- Zonal mass flux strengthens and meridional mass flux weakens;
- Warm Pool becomes stronger and meridionally wider;
- Cold Tongue becomes stronger and westward-extending.
- The factors feedback as below:

Factor	IPA and OEP	PSB and ISB
Surface wind convergence	Convergent	Divergent
Surface wind speed	Decreasing	Increasing
SST	Warmer	Colder
Poleward SST ascendent	Decreasing in IPA	Increasing
Precipitation (cloud)	Increasing	Decreasing
Total heat	Decreasing	Increasing
Latent heat	Increasing	Decreasing
Solar radiation	Decreasing	Increasing
Sensible heat + longwave	Increasing	Decreasing
Poleward shortwave ascendent	Increasing in IPA	Decreasing

During El Niño the above responses are generally reversed:
- Walker Circulation weakens and migrates eastward;
- Hadley circulation becomes stronger and more meridionally extended;
- Zonal mass flux weakens and meridional mass flux strengthens;
- Warm Pool becomes weaker and meridionally narrower;
- Cold Tongue becomes weaker and eastward-retreating.

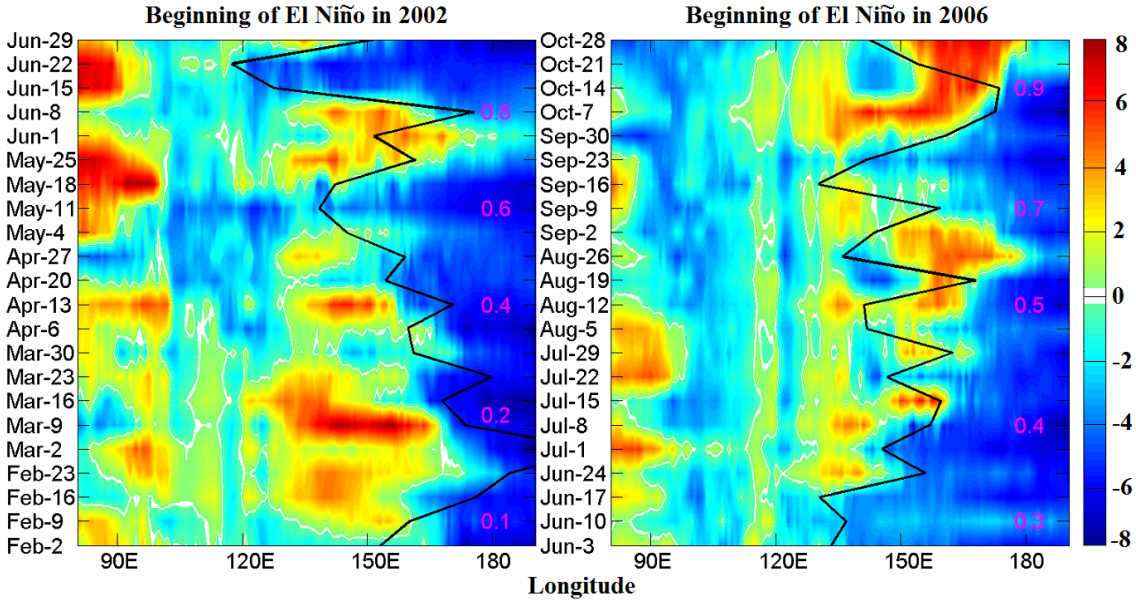

Fig. 4. The weekly averaged WCP (degrees; black line) and zonal wind within 5°S–5°N (m s^{-1}; colored contour) at the beginning of two El Niño events that started in June 2002 and August 2006, respectively. Wind was obtained from daily QuickSCAT surface winds from the NASA Ocean Vector Winds Science Team. The pink numbers are the monthly Niño3.4 SST anomalies obtained from the NOAA/National Weather Service and the NCEP/Climate Prediction Center.

this, the investigator can say that the left hand helps to move one book.

The key for LOAM to provide accurate simulations (e.g. correlation between the simulated and observed Niño SSTs is higher than 0.9 for the 288 months from 1979 to 2002) is that the observed and accurately com-

puted monthly anomalies and climatological means of FN (N=1–6) are used to drive LOAM. The basic seasonality and variations of FN have been included into LOAM at least on the interannual temporal scale.

Figures 5–8 were produced for the ENSO analysis in this section. Figure 5 depicts the mean mass streamfunction and the flux vectors (i.e. the product of wind and air density) of Walker (in an x–z plane) and Hadley (in a y–z plane) circulations averaged from September to the next February in eight individual El Niño and La Niña years 1950–2003. Figure 6 depicts the mass flux and its meridional component in an x–y plane averaged from October to the following February in all the El Niño and La Niña years 1950–2007 (both anomaly and mean), as well as in all the years 1950–2007 (mean), with seasonal signals removed from the anomaly. The patterns of ENSO feedback factors and their induced SST anomalies during December to February of El Niño and La Niña years are plotted in Fig. 7. The standard deviations of factor-feedback SSTs and their ratios to the standard deviation of the observed SST are given in Fig. 8. The basic feedbacks are summarized below.

6.1 *The general SST-feedback pattern of ENSO-feedback factors*

Walker circulations in both the Pacific and Indian Oceans become weaker (in 1997/98 El Niño; WCI = -0.01 kg s^{-1} m^{-1}; the least of the eight El Niño events), and the position of Walker cells moves eastward, especially in the Indian Ocean (WCI-WCP correlation = -0.405). Hadley circulations in both the Northern and Southern Hemispheres get stronger, and the position of the Hadley cells moves toward the Equator, or the Hadley cells extend less toward the poles. The WCI and HCI change oppositely, with a negative correlation (-0.636) and with the WCI lagging by approximately one month, during the El Niño phase (columns 1 and 3 of Fig. 5 for eight individual El Niño events 1950–2003, and Table 2) as compared with the La Niña phase during which the opposite of the above is generally the case (columns 2 and 4 of Fig. 5 for eight individual La Niña events 1950–2003, and Table 2).

Corresponding to the weakened (strengthened) general Walker (Hadley) circulations during the El Niño phase, the averaged zonal (meridional) mass flux at the bottom (100 000 Pa) of the troposphere over the tropical Indian and Pacific Oceans becomes weaker (stronger) by up to approximately 20% (first row and left column of Fig. 6) relative to the total mean mass flux that is dominated by easterlies (trade winds) and is transported toward the Equator (third row and left column of Fig. 6). The opposite of the above is generally the case during the La Niña phase (second row and left column of Fig. 6). The total mass flux at the bottom of the troposphere changes spatially, that is, mass flux over the tropical Indian or east Pacific Oceans is stronger in the Southern Hemisphere than in the Northern Hemisphere (3.7 kg s^{-1} m^{-2} vs. 2.9 kg s^{-1} m^{-2}, or 6.4 kg s^{-1} m^{-2} vs. 4.0 kg s^{-1} m^{-2}), while mass flux over the tropical west and middle Pacific Oceans is weaker in the Southern Hemisphere than in the Northern Hemisphere (3.1 kg s^{-1} m^{-2} vs. 5.9 kg s^{-1} m^{-2}). The size of the total mass flux does not change much (<9% over the separated tropical regions or <2.5% over the entire tropical region in Fig. 6) between El Niño and La Niña phases. What change is there in the direction of the total mass flux? At the top (20 000 Pa) of the troposphere over the tropical Indian and Pacific Oceans (right column of Fig. 6), the westerly dominates in the zones of 15°–30°N. During the El Niño phase, the meridional mass flux anomaly is toward the equator over the tropical Indian and east Pacific Oceans, but toward the poles over the tropical west and middle Pacific Oceans; the zonal mass flux anomaly is eastward over the Indian and Pacific Oceans, except the region within 15°S–15°N over the Pacific Ocean where it is westward. These processes are basically reversed during the La Niña phase. Between El Niño and La Niña phases, the size of the mean mass flux changes by 29%–37% over the separated tropical Indian Ocean, by 6%–13% over the separated tropical Pacific Ocean, and by <14% over the entire tropical Indian and Pacific Oceans.

The circulation changes are directly related to ENSO-feedback factors. During the El Niño phase (columns 1 and 3 of Fig. 7), an enhanced convergence of surface wind stress is accompanied with a strengthened meridional (toward the equator) but weakened zonal surface wind, and leads to warmer SST in the PSB and ISB; an enhanced divergence of surface wind stress is accompanied with intensified Hadley circulation and reduces SST in the IPA and OEP. Via heat exchange between the sea surface and air, SST and wind patterns directly influence the total heat flux that decreases in the PSB and ISB with increased SST and wind convergence while increasing within the IPA and OEP with increased SST and wind divergence. The total heat flux has a negative feedback on SST and decreases SST in the PSB and ISB while increasing SST in the IPA and OEP. Two major heat sources (i.e. solar radiation and latent heat) basically counteract one another. In the OEP and especially in PSB regions where the surface wind converges, the latent heat flux increases to produce a positive SSTA, but shortwave radiation decreases to induce a negative SSTA. Longwave radiation plus sensible heat has

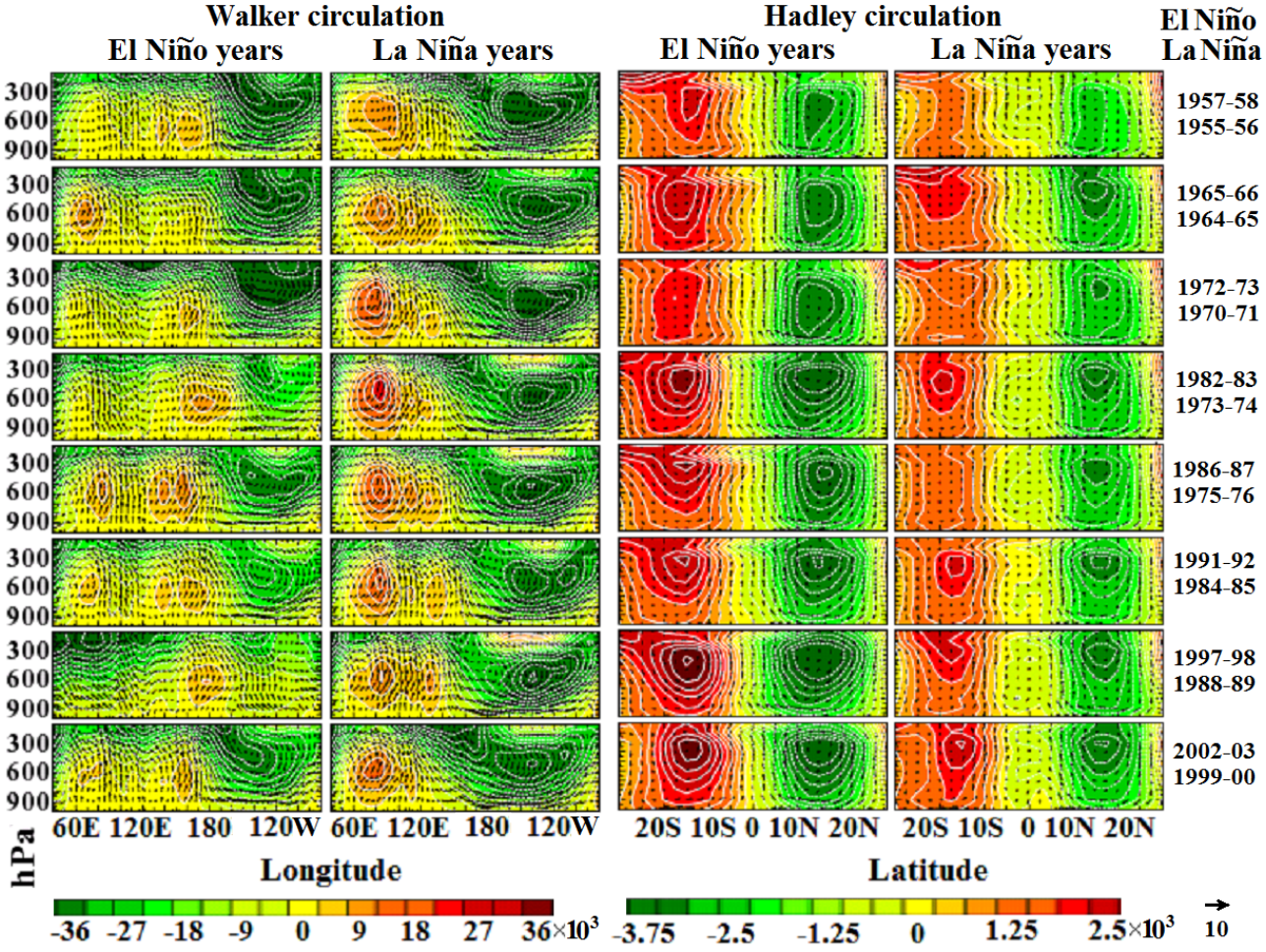

Fig. 5. The mean mass streamfunction (kg s^{-1} m^{-1}; see text) and the flux vectors (kg s^{-1} m^{-2}; the product of wind and air density) of Walker (first and second columns; averaged within 5°S–5°N) and Hadley (third and fourth columns; averaged within 50°E–100°W) circulations averaged from September to the next February, for El Niño (first and third columns) and La Niña (second and fourth columns) years based on monthly NCEP reanalysis data for 1950–2003. The individual El Niño and La Niña years in rows are listed on the right-hand side of the frames.

a similar pattern to that of wind stress convergence. Increased precipitation increases SST in the PSB region, while decreased precipitation reduces SST in the IPA and OEP regions by changing local vertical mixing (the more precipitation, the weaker the local vertical mixing). In these feedbacks, wind stress convergence, and therefore clouds, link dynamic processes with heating processes by changing the wind field (latent heat), SST, and solar radiation. The zonal and meridional gradients of SST correspondingly change with SST. The zonal contrast of equatorial SST is reduced with a higher Niño SST, and the Walker circulation is weakened and moves eastward. The relatively warmer tropical surface ocean (e.g. with a weakened cold tongue and an eastward extended warm pool, produces a relatively stronger meridional SST contrast (a weakened poleward ascendant for SST, for example, in Niño3.4) and strengthens the Hadley circulation (ascendant here refers to a negative gradient). During the La Niña phase (columns 2 and 4 of Figs. 7), the opposite of the above is generally the case owing to the westward migration and enhancement of the Walker circulation. One exception is that SST induced by longwave radiation plus sensible heat changes in a complicated way and with small amplitude. High correlation coefficients support the above analysis, as follows: 0.808 between the WCI and the meridional ascent of SST in Niño3.4; −0.731 between the WCI and the meridional ascent of shortwave radiation in Niño3.4; 0.462 between the WCI and the WPI; and −0.885 between the WCI and the CTP, based on monthly data and a simulated SST between 1979 and 2007.

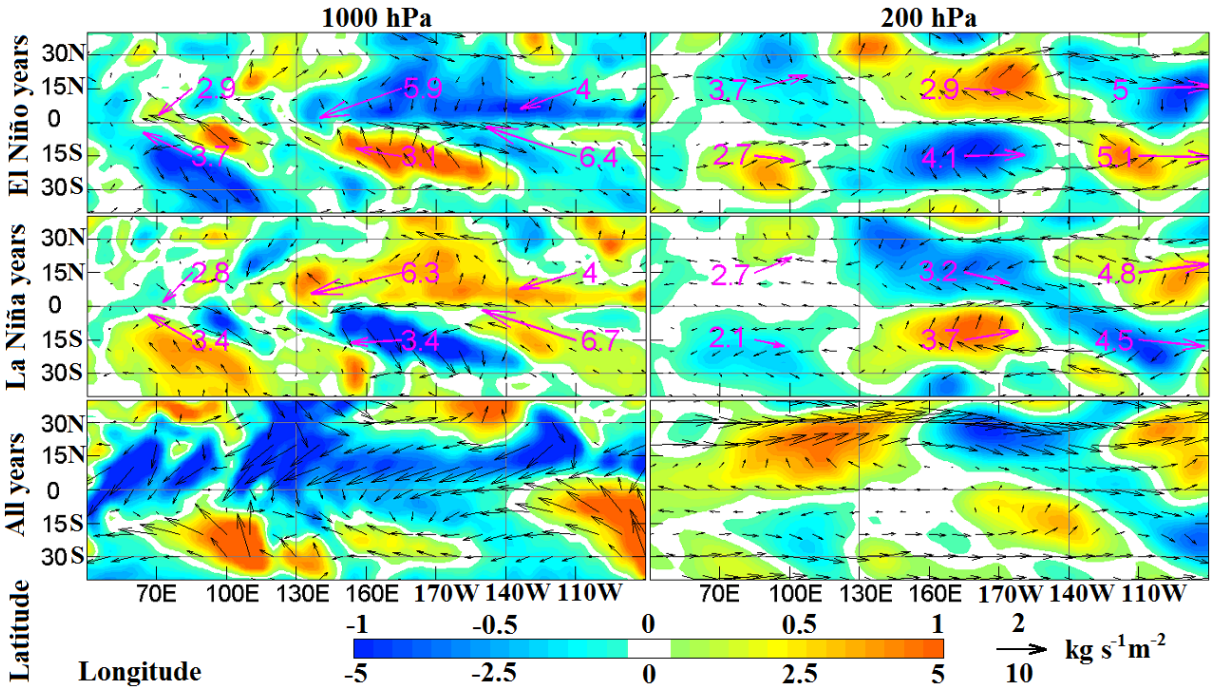

Fig. 6. The mass flux (kg s^{-1} m^{-2}) vectors (arrow) and meridional components (colored contour) averaged from October to the following February of El Niño, La Niña and all years plotted in the first, second and third row, respectively. With seasonal signals removed, the colored contour and black arrows in the first and second row are mass flux anomalies relative to the climatological mean mass flux from 1950 to 2007 plotted in the third row. The pink arrows are mean mass flux vectors with their sizes given by the pink numbers near their tails, averaged for the same period as the anomalies were and averaged within the six rectangular regions encircled by the grey lines. The left/right column is averaged at 100 000/20 000 Pa. The scales above/below the color bar and the black arrow are for the anomalies (rows 1 and 2)/mean (row 3). The mass flux (wind times density) was computed from the monthly NCEP reanalysis of wind and temperature at 100 000 and 20 000 Pa using ideal gas law. El Niño and La Niña years are defined in section 5 and Fig. 2.

6.2 *Temporal WCI feedback within the warm pool and* Niño 3.4

Here, the six prominent SST-feedbacks mentioned above are analyzed using the WCI as ENSO index. Feedbacks, as well as their feedback properties, are listed in Table 1.

In the warm pool, latent heat, sensible heat plus longwave radiation, wind stress convergence, and warm pool intensity, all associated with wind and SST, have a leading (active) positive feedback on the WCI, with lead times of approximately 3, 2, 3, and 3 months, respectively (the 12th, 16th, 20th, and 7th rows of Table 1). On the contrary, shortwave radiation and precipitation cause a 1–2-month lagging, both negative and positive, feedback on the WCI (the 14th and 18th rows of Table 1), respectively. The sign of the feedback directly depends on clouds (or, wind divergence). The total heat (the composite sum of all types of heat) over the warm pool region acts to intensify the Walker circulation with an approximate 10-month leading positive WCI-feedback (10th row of Table 1), which correspondingly increases the local SST, wind convergence, and cloud coverage. As a result of corresponding reductions in shortwave and sensible heat due to increases in cloud coverage and SST, a three-month lagging, negative WCI-feedback develops (9th row of Table 1).

In Niño3.4, latent heat has a one-month leading negative WCI-feedback (13th row of Table 1), and the poleward-shortwave/ SST ascendant has a one-month leading negative/positive WCI-feedback, while all other feedback factors lag by up to three months.

Leading by 2–10 months, WCI-feedbacks from heat fluxes and wind convergence become more significant and active within one year in the warm pool than in the Niño3.4 region.

6.3 *The SST contribution of ENSO-feedback factors*

Wind stress contributes to SST mainly within the PSB where the thermocline is shallower and SST is more sensitive to wind divergence (Fig. 8). In the

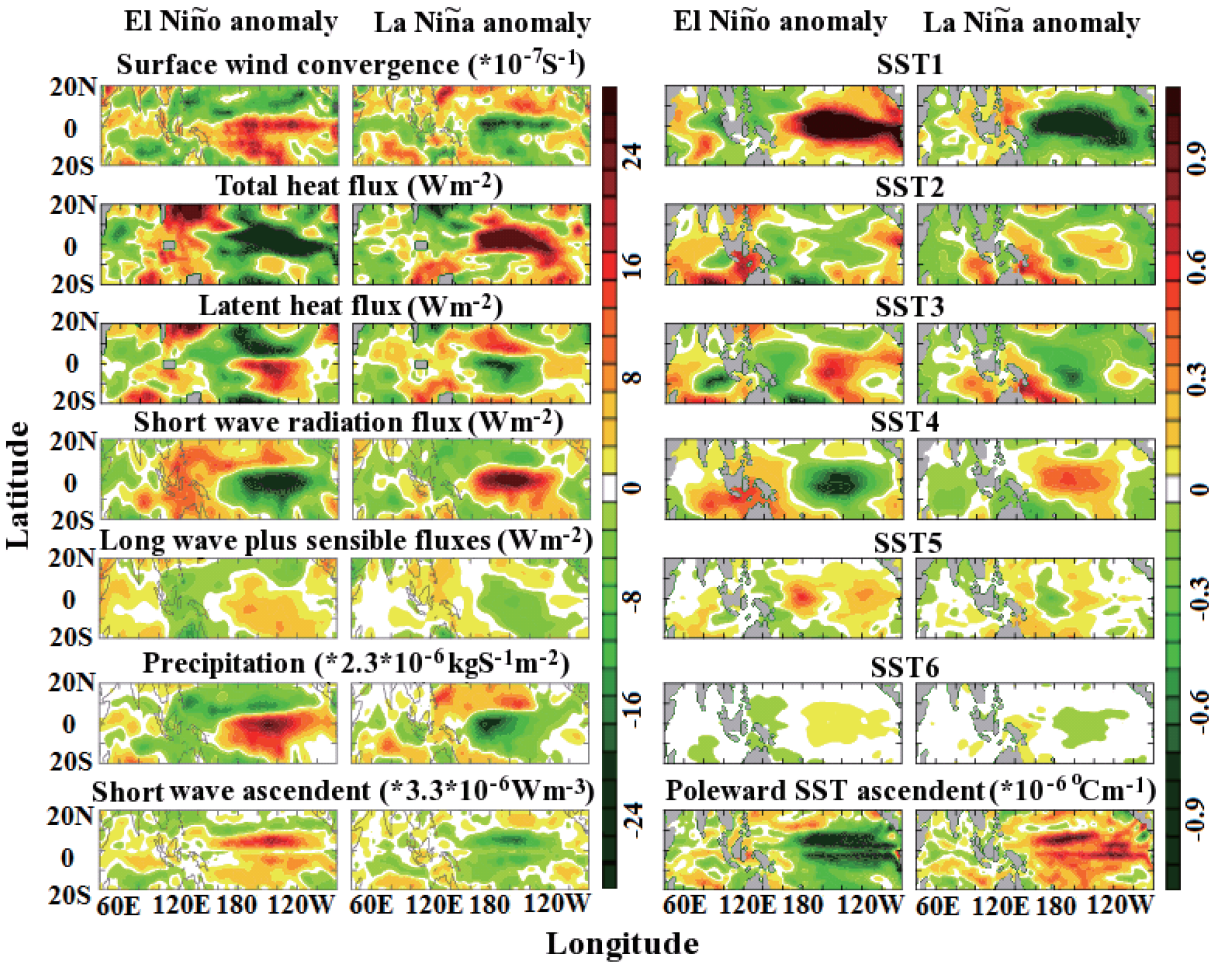

Fig. 7. Patterns of ENSO feedback factors (columns 1 and 2) as well as their induced SSTAs (columns 3 and 4) during December to February of El Niño years (columns 1 and 3) and La Niña years (columns 2 and 4) derived from 1979–2002 monthly LOAM-simulations and observations. SST1–SST6 are the SST anomalies (°C) induced by the wind stress, total heat flux, latent heat flux, shortwave radiation, longwave radiation plus sensible heat flux, and precipitation, respectively.

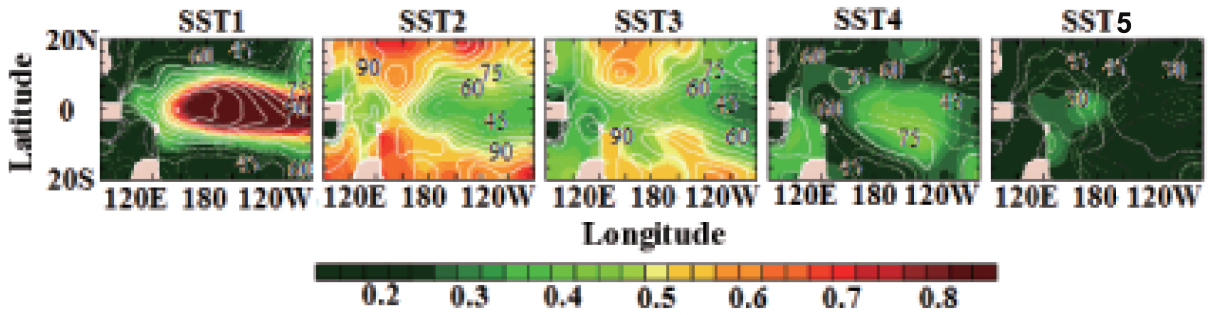

Fig. 8. The standard deviations of factor-feedback SSTs (°C; contoured) and their ratios (isolines, %; interval=15) to the standard deviation of the observed SST. SST1–SST5 are SSTAs induced by wind stress, total heat flux, latent heat flux, shortwave radiation, and longwave radiation plus sensible heat flux plus precipitation, respectively, based on 1979–2002 monthly LOAM-simulations and observations.

PSB, the convergent/divergent wind matches the positive/negative SSTA; the SSTR (the ratio of the standard deviation of the simulated to observed SSTs) of the wind stress can reach 100%–150%, and is maximized within the IPA–PSB transition area. In contrast, total heat contributes to SSTs mainly within the OEP and the warm pool where the thermocline is thicker and the SSTA induced by total heat is larger than those induced by wind stress. The SSTRs of total heat in these regions can reach 100%–165%. The SSTRs of latent heat, insolation, and longwave radiation plus sensible heat plus precipitation can reach 75%–165% within the OEP.

7. Summary and discussion

New ENSO indices were developed and numerical experiments were conducted to analyze and understand ENSO evolution. Computed from the mean circulation state in the large area above the planetary boundary layer (80 000–30 000 Pa), the new indices, with WCI as a typical one, do not rely on the geometrical shapes of the circulation cells and are not limited only by the properties at local areas such as at the surface, compared to the classic Southern Oscillation indices that are decided by sea level pressure difference between two stations, Tahiti and Darwin for SOI. Sea surface pressure cannot express Walker circulation accurately since Walker circulation is thermal and baroclinic. As compared to classic Southern Oscillation indices, the WCI generally has a higher correlation with SST and wind and better ENSO prognostic characteristics for SST and winds with a clear warm–cold phase relationship between the WCI anomaly and the Niño3.4 SST anomaly, conducing to ENSO analysis and prediction.

The new ENSO indices (i.e. WCI, WCP, HCI, WPI and CTP) developed in this work represent different aspects of atmospheric circulation in its position and intensity during ENSO. As discussed in more detail below, the integrity of atmospheric circulations was displayed with a high level of correlation among these aspects; new views on ENSO have been presented, e.g. the roles of westerly wind bursts in ENSO; and an answer provided as to whether or not the permanent warm mode will be present in the climate.

In an ENSO cycle, prominent ENSO-feedbacks (wind stress, heat fluxes, and precipitation) change temporally and spatially (as summarized in Tables 1 and 3). Wind stress significantly contributes to SST in the PSB region where the thermocline is shallow and SST is sensitive to wind divergence, and actively influences ENSO in the Warm Pool, leading the WCI by approximately three months. The wind stress-driven SSTA increases (decreases) within wind convergence (divergence) zones and is not strongly influenced by zonal wind anomalies, although the westerly wind anomaly corresponds to regions of convergence within the PSB. In contrast to wind stress, total heat flux influences the SSTA mainly in the OEP and IPA regions where the thermocline is thick, and increases the WCI by approximately 10 months in advance by enhancing atmospheric convection over the Warm Pool. However, it is reduced in approximately three months after the WCI reaches its maximum. Feedback mechanisms for the entire ENSO cycle can likely be inferred as the following. Feedbacks from total heat flux within the OEP and IPA regions intensify the Walker cell, increase local SST and wind convergence, forming a positive feedback in which the WCI lags convergence, latent heat, and sensible heat by approximately 2–3 months. Increased wind convergence leads to increased cloud coverage, which in turn leads to a local reduction in insolation, forming a negative feedback in which the WCI leads the shortwave radiation by approximately one month. The insolation reduction becomes dominant when the WCI approaches its maximum intensity, as it eventually causes the Walker circulation to weaken and move eastward, inducing positive westerly wind anomalies and increasing surface wind convergence and SST anomalies within the PSB. A phase change of ENSO cycle from a La Niña to an El Niño occurs with the weakened WCI. A couple of months before the Walker circulation becomes its strongest, the Hadley circulation adjusts and becomes weaker and less meridionally extended, with the WCI lagging the HCI and the poleward ascendant of the SST within Niño3.4 by approximately one month.

As part of holistic atmospheric circulation, various frequencies of zonal wind can be accompanied by or contribute to these circulations. The weakest and eastward moving Walker circulation coincides with the peak westerlies. Instead of being dominant during an ENSO cycle, noise-like westerly wind bursts are temporarily concomitant with atmospheric circulations. When the Walker circulation approaches its maximum positive intensity, instability will follow in the ENSO cycle where WCI-negative-feedbacks start to become dominant, resulting in the noise-like westerly wind burst. Concurrent weakening and the eastward propagation of the Pacific Walker cell and the Indian Walker cell permit the high-and-low-frequency westerly from the Indian branch near the surface to spread eastward toward the Pacific. Temporarily concomitant with atmospheric circulations, westerly wind bursts have no temporally persistent correlation with the high-frequency WCI, but briefly correlate with the high-frequency WCI a few weeks before/after

the Walker circulation reaches peak intensity to hinder/allow westerly wind bursts to occur. The general wind-WCI (i.e. zonal circulation) relationship permits a persistent and significant correlation between the WCI and zonal winds on an annual scale, as the low-frequency wind-WCI does.

In a sense, the transformation between La Niña and El Niño phases in an ENSO cycle generally accompanies with an adjustment of circulations. In this adjustment from, for example, La Niña to (normal state to) El Niño, Walker circulation intensity weakens from its maximum WCI and moves eastward while Hadley circulation intensity strengthens and meridionally extends. Correspondingly, the zonal wind component weakens and the meridional wind component strengthens. All the factors that influence the direction of circulation (or momentum) will influence the ENSO pattern of La Niña, or normal state, or El Niño. Other studies have found that there is considerable momentum accumulation inside the atmosphere and oceans under the tidal attraction of the Sun and Moon. This momentum accumulation varies temporally with multiple climatic rhythms and spatially with the structure of the observed weather and climate (Wang et al., 2012; Wang et al., 2012). The lasting and stable westward momentum accumulation in the tropical region helps maintain an ENSO cycle with a longer La Niña phase, making the La Niña-like pattern dominant during the ENSO cycle to maintain a "normal" instead of "warm" ENSO mode, as suggested by paleoclimate studies (Koutavas et al., 2002; Wara et al., 2005). The longer La Niña phase in an ENSO cycle is also supported by a positive feedback between SST and circulation: lower SST within the cold tongue corresponds to a stronger Walker circulation and a larger zonal equatorial SST contrast (SST in warm pool change less) to enhance the stronger Walker circulation and further decreases SST within the cold tongue, forming a persistent positive feedback to maintain the La Niña phase.

Secondary ENSO contributions may not be omitted over a larger time-space. Prominent ENSO feedbacks occur during mature El Niño and La Niña phases. For the majority of the studied time-space (77%–99% of the IPA and 60%–98% of the PSB during the period 1979–2002), variations of the prominent factors (wind stress, heat flux, and precipitation) were only approximately 20% of their maximum magnitudes, and their SST contribution was less than 20% of their maximum SST contribution (Fig. 9). The wind and total heat flux, as well as the two largest heating terms (latent heat and shortwave radiation) counter-

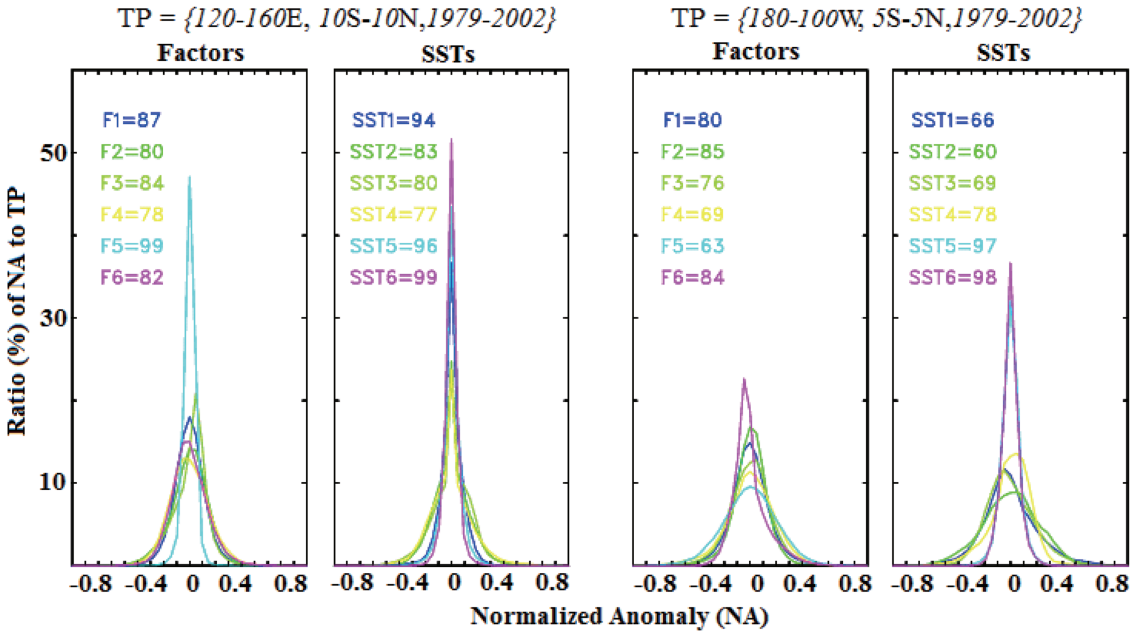

Fig. 9. The time-space (TP) distribution of normalized ENSO-feedback factors (F1–F6; columns 1 and 3), as well as their induced SST anomalies (SST1–SST6; columns 2 and 4). F1–F6 represent wind stress, total heat flux, latent heat flux, shortwave radiation, longwave radiation plus sensible heat flux, and precipitation, respectively. The values following the Fn or SSTn (n = 1–6) are TP percent, where the size of the normalized Fn or SSTn is less than 0.2 for the entire TP within (10°S–10°N, 120°–160°E; 1979–2002) (columns 1 and 2) or (5°S–5°N, 180°–100°W; 1979–2002) (columns 3 and 4). The data were based on 1979–2002 monthly LOAM simulations and observations.

act one another and induce different SST-feedbacks during El Niño and La Niña. Therefore, it is reasonable to hypothesize that additional secondary factors must contribute to ENSO through long-term accumulation (e.g., Stenchikov and Robock, 1995; Boulanger, 2001; Wang et al., 2011; Wang et al., 2012; Wang et al., 2012) since "ENSO is a very pronounced climate variability at the interannual time scale", as pointed out by one of the anonymous reviewers of this paper.

Acknowledgements. This research is supported by public science and technology research funds projects of ocean (Grant No. 201005019). The first author thanks Dr. Dale HAIDVOGEL (Rutgers University, NJ) for his support. All authors thanks Editors Riyu LU and Xiayu YUAN, copyeditor Colin SMITH, the anonymous reviewers for their useful comments on the manuscript.

REFERENCES

Boulanger, J. P., 2001: Role of non-linear oceanic processes in the response to westerly wind events: New implication for the 1997 El Niño. *Geophys. Res. Lett.*, **28**, 1603–1606.

Chelton, D. B., 1983: Effects of sampling errors in statistical estimation. *Deep-Sea Res.*, **30**, 1083–1101.

Chen, D., L. M. Rothstein, and A. J. Busalacchi, 1994: A hybrid vertical mixing scheme and its application to tropical ocean models. *J. Phys. Oceanogr.*, 24, 2156–2179.

Cox, P., and C. Jones, 2008: Illuminating the modern dance of climate and CO_2. *Science*, **321**, 1642–1644.

Ding, Y. H., and Z. Q. Zhang, 2000: On westerly wind bursts in equatorial western Pacific before and during the onset and initial development phases of ENSO. *Acta Meteorologica Sinica*, **14**(4), 385–401.

Emery, W. J., and R. E. Thomson, 1998: *Data Analysis Methods in Physical Oceanography.* 1st ed. Greg Publishing, 634pp.

Gent, P. R., and M. A. Cane, 1989: A reduced gravity, primitive equation model of the upper equatorial ocean. *J. Comput. Phys.*, **81**, 444–480.

Grove, R. H., 1998: Global Impact of the 1789–93 El Niño. *Nature*, **393**, 318–319.

Hadley, G., 1735: On the cause of the general trade winds. *Phil. Trans. Roy. Soc.*, **34**, 58–62.

Harrison, D. E., and G. A.Vecchi, 1997: Westerly wind events in the tropical Pacific. 1986–95. *J. Climate*, **10**, 3131–3156.

Holton, J. R., 1992: An introduction to dynamic meteorology. 3rd ed. *Academic Press*, 511pp.

Keen. R. A., 1982: The role of cross-equatorial tropical cyclone pairs in the Southern Oscillation. *Mon. Wea. Rev.*, **110**, 1405–1416.

Koutavas, A., L. S. Jean, T. M. Marchitto, and J. P. Sachs, 2002: El Niño–Like pattern in ice age Tropical Pacific Sea surface temperature. *Science*, **297**, 226–229.

Latif, M., J. Biercamp, and H. von Storch, 1988: The response of a coupled ocean–atmosphere general circulation model to wind bursts. *J. Atmos. Sci.*, **45**, 964–979.

Lau, K. M., and P. H. Chan, 1986: The 40–50 day oscillation and the El Niño/Southern Oscillation: A new perspective. *J. Atmos. Sci.*, **67**, 533–534.

Lau, K. M., and C. H. Sui, 1997: Mechanisms of short-term sea surface temperature regulation: Observation during TOGA COARE. *J. Climate*, **10**, 465–472.

Lean, J. L., and D. H. Rind, 2008: How natural and anthropogenic influences alter global and regional surface temperatures: 1889 to 2006. *Geophys. Res. Lett.*, **35**, L18701, doi: 10.1029/2008GL034864.

Lorenz, E. N., 1971: An N-cycle time differencing scheme for stepwise numerical integration. *Mon. Wea. Rev.*, **99**, 644–648.

McPhaden, M. J., and S. P. Hayes, 1991: On the variability of winds, sea surface temperature, and surface layer heat content in the western equatorial Pacific. *J. Geophys. Res.*, **96** (Suppl.), 3331–3342.

Moore, A. M., and R. Kleeman, 1999: Stochastic forcing of ENSO by the intraseasonal oscillation. *J. Climate*, **12**, 1199–1220.

Perigaud, C. M., and C. Cassou, 2000: Importance of oceanic decadal trends and westerly wind bursts for forecasting El Niño. *Geophys. Res. Lett.*, **27**, 389–392.

Seager, R., and M. B. Blumenthal, 1994: Modeling tropical Pacific sea surface temperature with satellite-derived solar radiative forcing. *J. Climate*, **7**, 1943–1957.

Shapiro, R., 1970: Smoothing, filtering, and boundary effects. *Rev. Geophys. Space Phys.*, **8**, 359–387.

Stenchikov, G. L., and A. Robock, 1995: Diurnal asymmetry of climatic response to increased CO_2 and aerosols: Forcings and feedbacks. *J. Geophys. Res.*, **100**, 26211–26227.

Walker, G., 1923: Correlation in seasonal variation of weather. VIII. A preliminary study of world weather. *Memoirs of the Indian Meteorological Department*, **24**, 75–131.

Wallace, J. M., and P. V. Hobbs, 2006: *Atmospheric science — An introductory survey.* 2nd Ed. Academic Press, 483pp.

Wang, B., and Z. Fang, 2000: Impacts of shortwave radiation forcing on ENSO: A study with a coupled tropical ocean-atmosphere model. *Climate Dyn.*, 677–691.

Wang, M., S. Ghan, M. Ovchinnikov, X. Liu, R. Easter, E. Kassianov, Y. Qian, and H. Morrison, 2011: Aerosol indirect effects in a multiscale aerosol-climate model PNNL-MMF. *Atmos. Chem. Phys.*, **11**, 5431–5455, doi: 10.5194/acp-11-5431-2011.

Wang, Z., D. Wu, X., Song, X., Chen, and S. Nicholls, 2012: Sun-moon gravitation induced wave characteristics and climate variation. *J. Geophys. Res.*, **117**, D07102, doi: 10.1029/2011JD016967.

Wara, M. W., A. C. Ravelo, and L. D. Margaret, 2005: Permanent El Niño–like conditions during the pliocene warm period. *Science*, **309**, 758–761.